Silicon-Based Photonic Crystals**

By *Albert Birner*, *Ralf B. Wehrspohn*, *Ulrich M. Gösele*,* and *Kurt Busch*

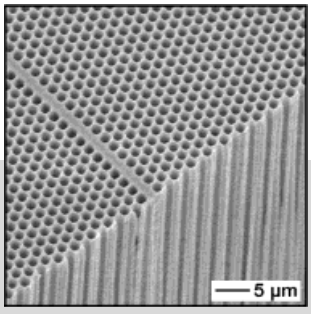

Photonic crystals can be thought of as optical analogues of semiconductors. Here recent advances in photonic crystals based on silicon are reviewed. After summarizing the theory of photonic bandgap materials, the preparation and linear optical properties of 1D, 2D, and 3D silicon-based photonic crystals are discussed. Laterally structured porous silicon with a defect line is shown in the Figure.

1. Introduction

In semiconductors electrons propagate in a periodic potential, which originates from the atomic lattice. This modifies the dispersion relation of free electrons and a band structure with a bandgap occurs in the case of semiconductors. The incorporation of electrically active defects allows the manipulation of the electronic properties, which gave birth to a large variety of electronic devices. There are distinct electrical and electro-optical properties of the different semiconductor materials, the dominant and most studied semiconductor being silicon.

For more than ten years, the optical analogues to electronic semiconductors, the so-called photonic crystals, have been the subject of intense international research efforts. Photonic crystals are materials with a periodically varying index of refraction. This allows the control of the propagation of electromagnetic waves, similar to electrons in a semiconductor crystal. By analogy with semiconductors, the periodicity of the underlying lattice structure is of the same order of magnitude as the wavelength of the electromagnetic radiation.

[*] Prof. U. M. Gösele, Dr. A. Birner,[+] Dr. R. B. Wehrspohn
Max-Planck-Institut für Mikrostrukturphysik
Weinberg 2, D-06120 Halle (Germany)
E-mail: goesele@mpi-halle.de

Dr. K. Busch
Institut für Theorie der Kondensierten Materie, Universität Karlsruhe
PO Box 6980, D-76128 Karlsruhe (Germany)

[+] Current address: Infineon Technologies, Memory Products, D-01099 Dresden, Germany.

[**] The authors are indebted to Drs. Volker Lehmann, Stefan Ottow, and Ulrike Grüning (Siemens Corp.) and Prof. Helmut Föll and co-workers (University of Kiel) for their essential help in the technological realization of the macroporous structures and to Prof. Wolfram Hergert (Martin-Luther University, Halle), Dr. Reinald Hillebrand, Dr. Frank Müller, Jörg Schilling, and Sven Matthias for collaboration and discussions in the area of photonic crystals. We gratefully acknowledge fruitful cooperation with the Universities of Toronto and Constance (Germany) and the MIT as well as financial support from the Deutsche Forschungsgemeinschaft under grant Bu 1107/2-1.

Despite the far-reaching analogies between electronic waves in semiconductors and electromagnetic waves in photonic crystals, there are pronounced differences between the two as is noticeable from the corresponding equations of motion. Electrons are described by a scalar wavefield. In contrast, the electromagnetic field is vectorial by nature. Furthermore, the time-independent Schrödinger equation allows solutions with negative energy eigenvalues, whereas the corresponding wave equation in electrodynamics contains only the square of the eigenfrequencies, hence negative eigenvalues are excluded from the outset. It may be inferred from the few photonic crystals that appear in nature, in contrast to ubiquitous semiconductor materials, that these differences have a disadvantageous effect on the likelihood of the formation of photonic bandgaps. From the multitude of the optical phenomena only, for example, the colorful speckles of opals, some crystallites on the wings of butterflies and the spine of the seamouse[1] can be attributed to photonic crystal effects. Due to the extreme requirements of miniaturization, substantial progress in nanotechnology has recently allowed the artificial manufacturing of photonic crystals for optical frequencies to be considered in a controlled way. Therefore, photonic crystals may play a key role in the realization of novel integrated optical devices. Besides important technological aspects, photonic crystals provide entirely new avenues of basic research through their potential in controlling the propagation of electromagnetic waves, in particular in the field of nonlinear and quantum optics.[2]

There are many types of dielectric materials for photonic crystals under current investigation: group II–VI, III–V, and IV semiconductors as well as oxides, polymers, and metallodielectric structures. In this review, we will focus on recent advances in silicon-based photonic crystals, which is the dominant material in semiconductor industry. In Section 2, we will briefly review the theoretical basis of photonic bandgap materials. Then we will discuss preparational aspects of 1D, 2D, and 3D photonic crystals made out of silicon and present

  0935-9648/01/0603-0377 $ 17.50+.50/0

some linear optical properties of the photonic crystals. Finally, we give an outlook on dispersion-relation engineering and its impact on nonlinear and quantum optical properties of these photonic crystals.

2. Theory

The simplest way to calculate photonic band structures is to apply the methods of electronic band structure calculations.

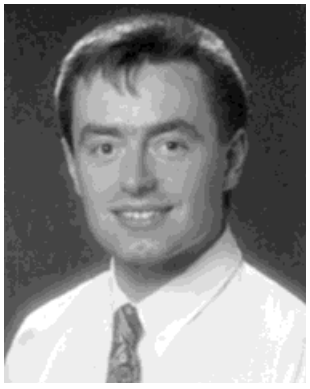

Albert Birner received his diploma in physics at the University of Regensburg in 1996 and his Ph.D. in physics from the Martin-Luther-University of Halle-Wittenberg, Germany. Dr. Birner has been an employee of Infineon Technologies AG in Dresden since October 1999. His R&D work is related to integration of innovative processes and process modules for future DRAM generations. His primary interests are in the fields of porous silicon, photonic crystals, photonics, and optics.

Ralf B. Wehrspohn received his diploma in physics at the University of Oldenburg in 1995. He then carried out a Ph.D. at the Ecole Polytechnique in France on thin film technology and electrochemistry. In 1998 he joined the Philips Research Laboratories in Redhill, UK, to work on thin film transistors for active-matrix liquid crystal displays (AMLCDs). Since the end of 1999 he has been responsible for the activities on photonic crystals and self-ordered porous materials at the Max Planck Institute of Microstructure Physics in Halle.

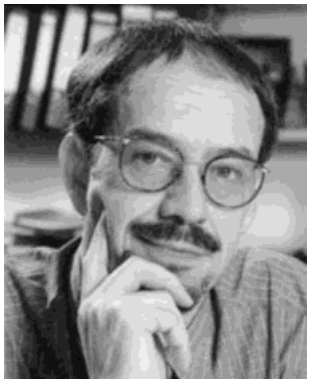

Ulrich M. Gösele has been a director at the Max Planck Institute of Microstructure Physics, Halle, Germany, since 1993. For many years he was a J.B. Duke Professor of Materials Science at Duke University in North Carolina. Prior to that he worked at the Siemens Research Laboratories in Munich. He has had visiting appointments at IBM's Watson Research Center, the NTT LSI Laboratories in Atsugi, Japan, and the Atomic Energy Board in South Africa. His research interests include defects and diffusion process in semiconductors, quantum effects in porous silicon, self-organized structure formation, semiconductor wafer bonding, and photonic crystals.

Kurt Busch is head of a junior research group (Emmy-Noether program of the Deutsche Forschungsgemeinschaft) at the Institute for Theory of Condensed Matter at the University of Karlsruhe (Germany). His research interests lie in light propagation in strongly scattering media and photonic crystals. His undergraduate and postgraduate training was at the University of Karlsruhe (Germany) and partly at the Iowa State University (Ames, USA). His professional experience has included working at Iowa State University (Ames, USA) and at the University of Toronto (Canada).

  0935-9648/01/0603-0378 $ 17.50+.50/0

ADVANCED MATERIALS

However, various adjustments are necessary to take into account the specific differences between photonic and conventional crystals. First, the electromagnetic field is inherently vectorial by nature, implying that scalar approximations are insufficient. Second, the "scattering potentials" of the dielectric atoms are known beforehand and do not have to be determined self-consistently.

In the following, it is outlined how the widely used plane wave method (PWM)[3] can be applied to the problem of photonic band structure computation. We consider the wave equation for a magnetic field H with harmonic time dependence for a 3D periodic array of scatterers. If the materials differ only in the dielectric but not in the magnetic permeability, we obtain the following wave equation by combining Maxwell's equations.

$$\nabla \times \left(\overleftrightarrow{\epsilon}^{-1}(\vec{r}) \nabla \times \vec{H}(\vec{r}) \right) - \frac{\omega^2}{c^2} \vec{H}(\vec{r}) = 0 \tag{1}$$

where ω are the eigenfrequencies and c the speed of light. The information about the structure of the photonic crystal is fully contained in the dielectric tensor $\overleftrightarrow{\epsilon}(\vec{r}) = \overleftrightarrow{\epsilon}(\vec{r} + \vec{R})$, which is periodic with respect to the set $\mathcal{R} = \{n_1\vec{a}_1 + n_2\vec{a}_2 + n_3\vec{a}_3; (n_1,n_2,n_3)\}$ of lattice vectors $\vec{R}$, which are generated by the primitive translations $\vec{a}_i$, $i = 1, 2, 3$. We discuss from the outset the general case of an anisotropic tensor. The special case of an isotropic medium can be obtained by replacing the dielectric tensor by a scalar times the unit tensor.

The photonic dispersion relation can be obtained straightforwardly by considering the wave equation (Eq. 1) in reciprocal space, i.e., the dual description of the crystal lattice. To this end, the periodic inverse dielectric tensor is expanded in a Fourier series on $\mathcal{G}$ the reciprocal (dual) lattice corresponding to $\mathcal{R}$:

$$\overleftrightarrow{\epsilon}^{-1}(\vec{r}) = \sum_{\vec{G} \in \mathcal{G}} \overleftrightarrow{\epsilon}^{-1}_{\vec{G}} \, e^{i\vec{G}\vec{r}} \tag{2}$$

where the Fourier coefficients $\overleftrightarrow{\epsilon}^{-1}_{\vec{G}} = (1/V)\int_V \mathrm{d}^3 r \overleftrightarrow{\epsilon}^{-1}(\vec{r}) e^{-i\vec{G}\vec{r}}$ are obtained through an integration over the Wigner–Seitz cell (WSC) whose volume we have designated by V. Using the Bloch–Flouquet theorem, the magnetic field may be expanded into the eigenfrequencies $h^{\lambda}_{\vec{G}}$ as

$$\vec{H}(\vec{r}) \equiv \vec{H}_{\vec{k}}(\vec{r}) = \sum_{\vec{G} \in \mathcal{G}} \sum_{\lambda=1}^{2} h^{\lambda}_{\vec{G}} \, \hat{e}^{\lambda}_{\vec{G}} \, e^{i(\vec{k}+\vec{G})\vec{r}} \tag{3}$$

Here, we utilized the fact that $\nabla \cdot \vec{H}(\vec{r}) = 0$, so that λ labels the two transverse polarizations for any plane wave such that the polarization unity vectors $\hat{e}^{\lambda=1,2}_{\vec{G}}$, $(\vec{k} + \vec{G})/|\vec{k} + \vec{G}|$ form an orthogonal triad. Due to the discrete translational symmetry of the lattice, the wave vector $\vec{k}$ labeling the solution may be restricted to lie in the first Brillouin zone (BZ). As a consequence, the dispersion relation in the infinitely extended momentum space is folded back onto the first BZ, introducing a discrete band index n. However, care must be exercised in identifying the irreducible part of the Brillouin zone (IBZ). The dielectric tensor in Equation 1 may have fewer rotational symmetries than the underlying lattice and consequently the IBZ for a photonic crystal containing anisotropic materials may be considerably larger than the IBZ for the corresponding isotropic crystal. Rather than dealing with an IBZ that changes from problem to problem, one can choose to work with the standard IBZ for the isotropic material and solve Equation 1 for all inequivalent transformations of the given dielectric tensor with respect to the rotational symmetries of the underlying lattice.[4]

Inserting Equations 2 and 3 into Equation 1 results in an infinite matrix eigenvalue problem

$$\sum_{\vec{G}' \in \mathcal{G}} \sum_{\lambda'=1}^{2} M^{\lambda\lambda'}_{\vec{G}\vec{G}'} \, h^{\lambda'}_{\vec{G}'} = \frac{\omega^2}{c^2} h^{\lambda}_{\vec{G}} \tag{4}$$

where the matrix elements $M^{\lambda\lambda'}_{\vec{G}\vec{G}'}$ are given by

$$M^{\lambda\lambda'}_{\vec{G}\vec{G}'} = |\vec{k} + \vec{G}|(\hat{e}^{\lambda}_{\vec{G}} \times \overleftrightarrow{\epsilon}^{-1}_{\vec{G}-\vec{G}'} \times \hat{e}^{\lambda'}_{\vec{G}'})|\vec{k} + \vec{G}'| \tag{5}$$

In order to obtain the photonic band and mode structure, Equation 4 has to be solved for both eigenvalues and eigenvectors which for a given wave vector $\vec{k}$ are labeled by the band index n. Then, the electric field corresponding to a given eigenfrequency $\omega_n(\vec{k})$, can be computed from Maxwell's equation

$$\vec{E}_{n\vec{k}}(\vec{r}) = -i \frac{c}{\omega_n(\vec{k})} \overleftrightarrow{\epsilon}^{-1}(\vec{r}) \nabla \times \vec{H}_{n\vec{k}}(\vec{r}) \tag{6}$$

The photonic dispersion relation gives rise to a photonic density of states (DOS), which plays a fundamental role in the understanding of the properties of a photonic crystal. The photonic DOS $N(\omega)$ is defined by "counting" all allowed states of the photonic crystal with a given frequency ω, i.e., by the sum of all bands and the integral over the first BZ of a Dirac-δ function

$$N(\omega) = \sum_{\mathrm{n}} \int_{BZ} \mathrm{d}^3 k \delta(\omega - \omega_n(\vec{\mathrm{k}})) \tag{7}$$

Figure 1 displays the band structure and densities of states of a hexagonal 2D photonic crystal, which have been computed via the methods outlined above. In 2D photonic crystals the two polarizations of the electromagnetic field decouple if we restrict ourselves to the propagation perpendicular to the axes of the air cylinders. We can thus consider the polarizations of the electric field parallel (E-polarization) and perpendicular (H-polarization) to the cylinder axis separately.[5] Figure 1b shows the corresponding 2D DOS. By analogy with electronic band structure calculations, flat bands in the band structure lead to large values of the DOS.

Transmission calculations through finite slabs of photonic crystalline material are usually based on finite difference time domain (FD-TD) methods[6] and the related transfer matrix method.[7] While these methods can handle disordered structures as well as ordered photonic crystals they also require considerable computational resources. For the special case of cylindrical[8] and spherical[9] geometries an efficient and accurate method based on multiple scattering has recently been developed, which enables the computation of transmission

  0935-9648/01/0603-0379 $ 17.50+.50/0

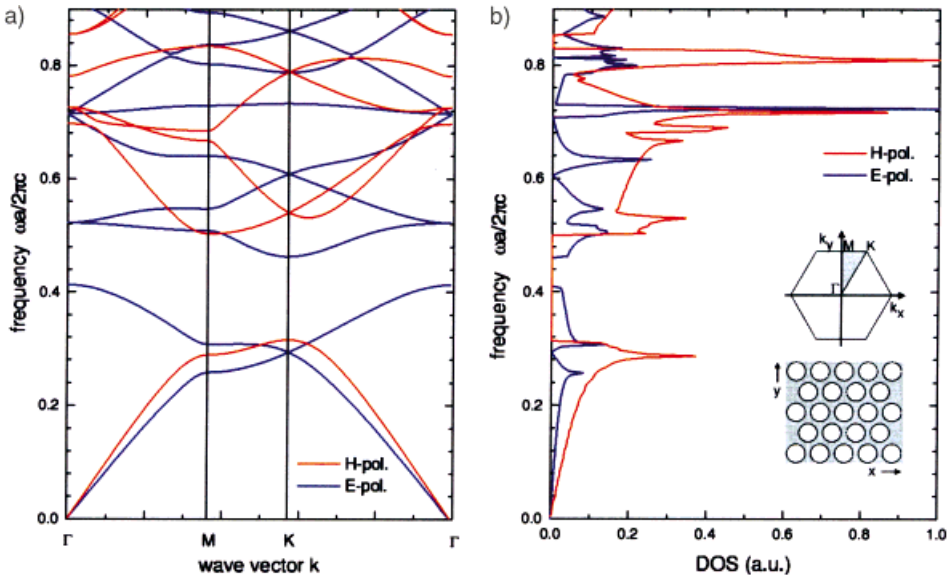

Fig. 1. Photonic band structure of a 2D silicon photonic crystal with a hexagonal arrangement of cylindrical air holes (a) and the corresponding frequency-dependent DOS (b). The inset schematically shows a hexagonal lattice and the corresponding reciprocal lattice. The irreducible part of the first BZ and the high-symmetry points Γ, M, and K are indicated.

through ordered and disordered slabs of cylinders and also allows a direct determination of the band structure of the infinite periodic system.

3. 1D Photonic Crystals

Dielectric mirrors (Bragg reflector) and interference filters were actually the first (1D) photonic crystals. However, they usually are not referred to as crystals because the name crystal is normally reserved for 2D or 3D structures. Typically, these 1D photonic crystals are prepared by layer-by-layer deposition of alternating materials. For example, a layered stack of TiO_2/SiO_2 deposited by sputtering techniques can be used as an optical coating for windows. For these 1D structures today's coating technology allows thin film stacks to be prepared on substrates larger than 3.2 m × 6 m. A stop gap in a desired spectral range can then be achieved by appropriately adjusting the dielectric contrast and the thickness ratios of the alternating layers. The classical layer-by-layer deposition has, however, the disadvantage that only discrete values of the dielectric constant are possible, in the simplest case two values. In Rugate filters[10] the discrete layer structure is replaced by a continuous modulation of the refractive index with depth. This has the beneficial effect that there are fewer sidelobes in the spectra and that one has a greater freedom for filter preparation. Rugate filters are more difficult to prepare with classical plasma-deposition systems since a smooth change from one stoichiometry to the other is technologically difficult to achieve. It has been shown that microporous silicon is a suitable candidate for the fabrication of Rugate filters as shown by Berger et al.[11] Due to the dependence of the porosity of the porous film (i.e., effective refractive index) on the anodization current, the dielectric contrast can be adjusted between 1.5 and 3. However, since the porous layers are still on the substrate and free-standing microporous layers are very fragile, this type of Rugate filter can only be used in reflection mode, i.e., as a Bragg reflector.

There are two problems with simple dielectric filters or mirrors for use in micro-optoelectronics. First, for an angle of incidence greater than a critical angle, light whose frequency lies in the bandgap of the 1D crystal can penetrate through the film (except for omnidirectional reflectors, which consist of very high index material[12]). Second, there is no guidance of the light, which lies energetically outside the photonic bandgap or within a defect band. Recently, an interesting approach has been pursued by the group of Kimerling[13] to create 1D integrated structures. A waveguide with a diameter of about 0.5 μm was structured on a silicon-on-insulator (SOI) substrate using X-ray lithography to provide a periodic arrangement of holes (Fig. 2). They omitted one pore in the center, which acts optically as a resonator having a drastically increased electromagnetic field at the defect site. At the reso-

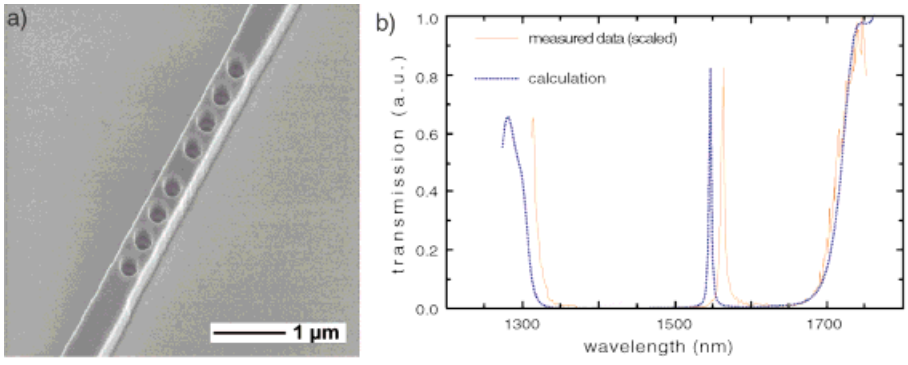

Fig. 2. SEM image of a 1D waveguiding structure made of silicon (a). By incorporating holes at periodic distances one yields a resonator-like functioning of the waveguide, as was demonstrated by transmission calculations (b) [13].

0935-9648/01/0603-0380 $ 17.50+.50/0

nance frequency, the transmitted intensity was measured to be about 80 % relative to the transmitted intensity outside the photonic bandgap (PBG). The volume of the resonant mode, being proportional to $(\lambda/2n)^3$, was estimated to be V = 0.055 μm^3. For the resonance at central wavelength λ_c and half-width $\Delta\lambda$, the value of the measured quality factor of the resonance $Q = \lambda_c/\Delta\lambda$ was about 265, slightly lower than the theoretical value of 280 obtained by numerical simulations. In a classical resonator, this quality factor Q describes the number of periods that a resonant wave packet spends within a cavity. Notice that this simple interpretation does not fully apply to the present situation, since here the average cavity length of $\lambda_c/2$ allows only the existence of a single (longitudinal) resonator mode.

4. 2D Photonic Crystals

If one retains periodicity in the *xy*-plane and lets the *z*-direction be homogeneous, one can describe the propagation within the *xy*-plane in terms of a band structure, which under suitable circumstances exhibits bandgaps in two dimensions (Fig. 1). We term such a structure a 2D photonic crystal. As discussed in Section 2, characteristic of such a 2D photonic crystal is the decoupling of the electromagnetic vector field into two scalar fields, one for each polarization. Since the two polarizations exhibit different behavior each 2D photonic crystal may be utilized to achieve polarization-dependent effects. 2D photonic crystals are much easier to fabricate than 3D structures, since well-known methods for the fabrication of columnar structures[14] may be easily modified for this purpose.

Initially, 2D photonic crystals were constructed either from macroscopic arrangements of sticks or from bundles of glass fibers, and subsequently studied in the microwave or infrared regime. A breakthrough has been achieved by Lehmann's group at Siemens Corp.[15] using their self-developed process of electrochemically growing ordered macropores in silicon. The structures obtained with this method for the first time showed a complete 2D bandgap in the near-infrared (near-IR) at a wavelength of about 4.9 μm. A complete 2D bandgap in this context means a direction- and polarization-independent bandgap for propagation that is confined to the plane of periodicity.[15] In the following we discuss exemplarily the optical properties of 2D photonic crystals based on macroporous silicon.

4.1. Preparation of Macroporous Silicon

A detailed description of the pore formation in macroporous silicon can be found elsewhere.[16–18] Here, we just give a short summary. First, an n-type silicon wafer with ⟨100⟩ orientation is prepatterned by photolithography. Subsequent alkaline etching produces inverted pyramids acting as pore seeds. Under anodic bias and backside illumination the wafer is then etched in hydrofluoric acid. The electronic holes generated by the illumination near the back surface diffuse through the whole wafer and promote the dissolution of silicon mainly at the pore tips. As a result, pores grow straight along the ⟨100⟩ direction with a very high aspect ratio. The spatial arrangement of these pores is controlled through the lithographic mask, whereas their diameter is controlled by the illumination intensity. With suitably adjusted parameters, variations of pore diameters both between neighboring pores and with depth may be minimized to negligible values.

For optical investigations or applications of such structures the porous silicon has to be processed further. The 2D photonic crystal has translational symmetry perpendicular to the pore axes. Therefore, analyzing the band structure requires the photons also to travel perpendicular to the pore axis. Investigations of the properties of defects demand access to the end of, e.g., a waveguide and require parts of the porous silicon to be removed with a precision of about one lattice constant, i.e., a precision of about 1 μm. To meet these specifications, a special microstructuring technique has been developed.[19] First, the pore walls are passivated by a thermal oxide and a chemical vapor deposited (CVD) nitride. Afterwards, an aluminum layer is sputtered onto the porous silicon and structured by conventional photolithography. Although the feature sizes of this second mask are in the 10 μm range, the precision of the structures and the alignment relative to the defects is better than 1 μm. In the opened window of the aluminum mask the passivating oxide and nitride are removed by chemical etching. In a subsequent isotropic plasma etching process the porous silicon in the areas without passivation is etched away, leading to the desired bar structure. The quality of this process is demonstrated in Figure 3, where a bar of porous silicon is shown that consists of about 22 pore layers. The transition from air to the 100 μm deep pores occurs within only one pore layer. By combining the above techniques, we obtain free-standing bars of porous silicon on a silicon sub-

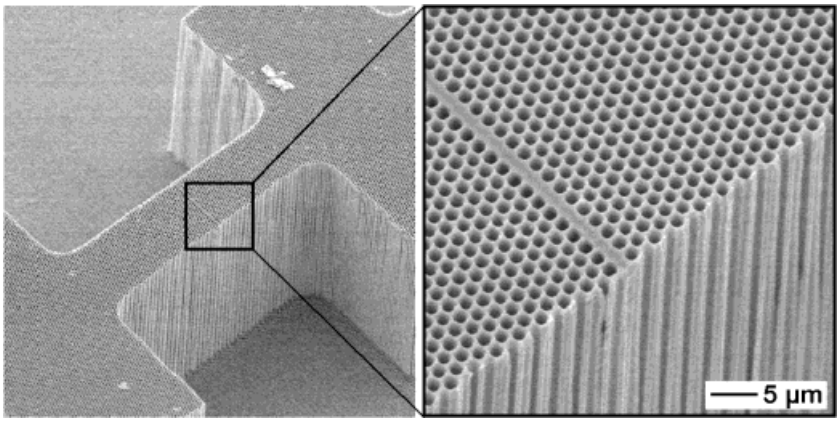

Fig. 3. Laterally structured porous silicon sample with a defect line. The H-like structure facilitates the positioning of a fiber for the coupling in and out of light. The pore separation is 1.5 μm and the height of the porous silicon is 100 μm.

0935-9648/01/0603-0381 $ 17.50+.50/0

strate that are 100 μm high, 2–200 μm wide, and several millimeters long. In addition, the bars may be aligned with the designed defect structures in the porous silicon.

4.2. Bulk Photonic Crystals

The processed macroporous Si samples described above are extremely well suited to investigating the optical properties of light traveling perpendicular to the pores. We have performed transmission measurements on such bars for different pore diameters, polarizations, and directions. In Figure 4 spectra of defect-free samples with two different pore diameters each

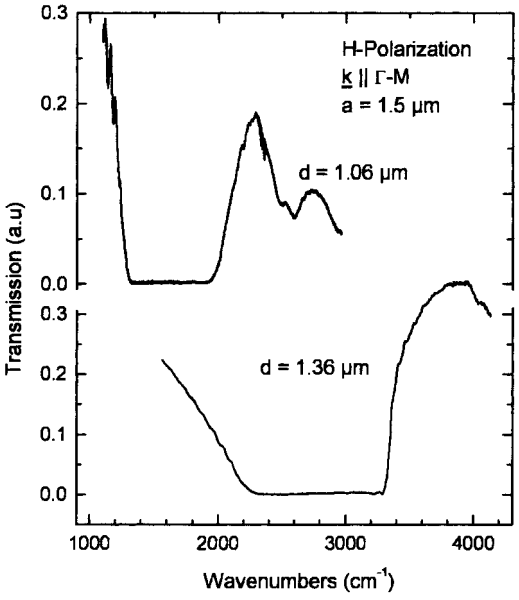

Fig. 4. Transmission spectra of two samples of 2D photonic crystals with different pore diameter d along the Γ–M direction, i.e., along the pore rows. The lattice constant a is 1.5 μm, the width of the porous silicon bar is 33 μm. The measurement is for H-polarized light, i.e., transverse electric (TE) polarization where the magnetic field is parallel to the pore axes.

consisting of 22 pore layers are shown for the Γ–M direction, H-polarization, and a lattice constant a of 1.5 μm. Depending on the pore diameter, the center of the stop-band shifts from 1650 cm^{-1} (6 μm wavelength) for a pore diameter of 1.06 μm up to 2800 cm^{-1} (3.6 μm wavelength) for 1.36 μm. Repeating this measurement for the other directions and for E-polarization, we find a complete gap centered at 3.2 μm for 1.36 μm pore diameter and no overlap of the different stop bands for the 1.06 μm sample. This is in good agreement with theoretical predictions for such structures.

In Figure 5 we present a map for the bandgaps resulting from such measurements for a whole set of samples with varying pore diameters (symbols) for a = 1.5 μm. For comparison, the theoretical predictions from a plane wave expansion method (see Sec. 2) are shown as solid lines. For the lower filling factors the agreement between theory and experiment is excellent. For very high porosities slight deviations occur, due to the difficulty in preparing and handling these very fragile

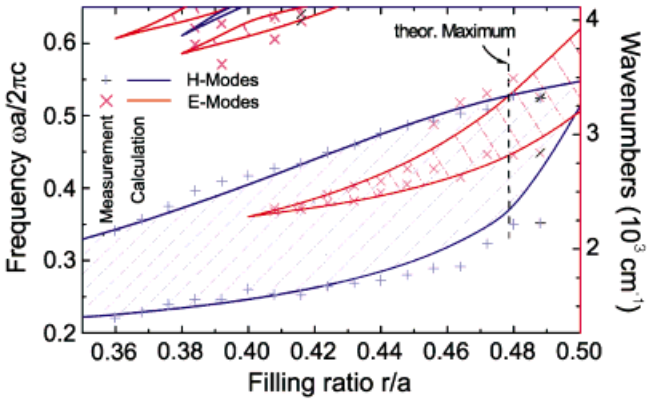

Fig. 5. Dependence of the observed bandgaps on polarization and filling factor (gap map) for a lattice constant a of 1.5 μm. Theoretical (solid lines) and experimental (symbols) values show very good agreement [20].

samples. Therefore, the observed discrepancies are the result of small differences between the real dimensions of the samples and the values used in the calculations.[20]

To obtain bandgaps in the opto-electronically interesting region of around 1.3 to 1.55 μm downscaling of the above-described triangular pore lattice is necessary. Recently, we have shown for the first time that it is possible to fabricate pores with a pitch of a = 0.5 μm (Fig. 6).[21] The pores fabricated had a radius r = 0.18 μm, resulting in an r/a ratio of 0.43 and a pore depth of 100 μm. To investigate the 2D bandgaps in the near-IR, we have performed reflection measurements similar to those of Rowson et al.[22] The resulting sample spectra are shown in Figure 6. Band structure calculations were performed using 967 plane waves. The shaded spectral ranges represent the theoretically expected regions of high reflectivity. They largely coincide with the bandgaps along the Γ–M direction. Figure 6 reveals good agreement between the theoretically predicted ranges of total reflection and the experimentally determined high reflectivity regions. From the calculated band structure a complete bandgap for E- and H-polarization is expected for the spectral range from 1.22 μm to 1.3 μm, thus incorporating the wavelengths of the second telecommunication window.

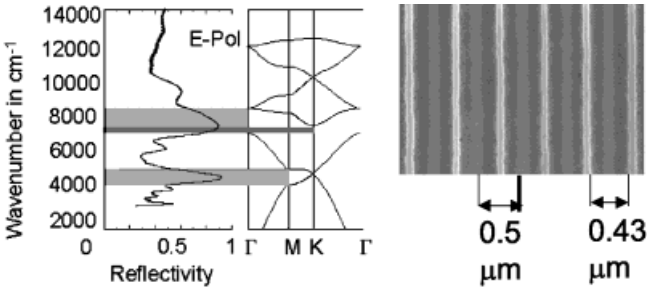

Fig. 6. Left: Measured reflectivity for the Γ–M direction and comparison with band structure calculations for E-polarization. The light-gray shaded regions correspond to regions of high reflectivity. The dark-gray shaded region corresponds to the complete 2D photonic bandgap at around 8000 cm^{-1} (1.25 μm). Right: Cross-sectional SEM image of a structure with a lattice constant of 500 nm and r/a of 0.43 [21].

0935-9648/01/0603-0382 $ 17.50+.50/0

4.3. Finite Photonic Crystals

For practical purposes finite photonic crystals are important. For a thin slab of a photonic crystal the light will no longer be totally reflected but a certain amount is transmitted. A band structure for such a thin crystal cannot be determined because of the lack of long-range periodicity. However the bandgap of the bulk crystal has to build up with growing number of crystal rows. Besides interesting physical properties, photonic crystals possess a considerable potential for opto-electronic applications. The incorporation of linearly extended defects leads to localized photonic states in the bandgap. Light can be guided through these waveguides, allowing high integration densities for opto-electronic components. However, coupling phenomena have to be understood for the defect design to adjust the minimum distance between two waveguides.

Transmission measurement were performed on 1–4 crystals rows of macroporous silicon using a tunable pulsed laser setup.[23] For comparison, calculations of the transmittance using the Sakoda approach were performed and a very good agreement with the experimental results was observed. Upon plotting the transmittance on a logarithmic scale against the penetrated crystal thickness a linear relationship is observed.[24] This reveals exponential decay of the transmission with increasing crystal thickness as expected from the case of bulk photonic crystal. From the slope a decay constant of about 10 dB per pore row can be derived for wavelengths deep within the gap. In summary, the bandgap of the bulk crystal is already perceptible for one crystal row. This can be ascribed to the strong refractive index contrast between the air pores and the silicon pore walls as well as to the high perfection of the investigated structures. For integrated defect structures, a minimum distance of about four crystal rows should be considered to avoid crosstalk between neighboring waveguides.

4.4. Defects in Photonic Crystals

If some etch pits are omitted by using a suitable mask for the photolithography, the electronic holes that are generated at the back side through illumination are consumed by the neighboring pores without influencing their position. The result of this procedure is a rather perfect structure with some missing pores at predefined positions, as shown in Figure 7 for

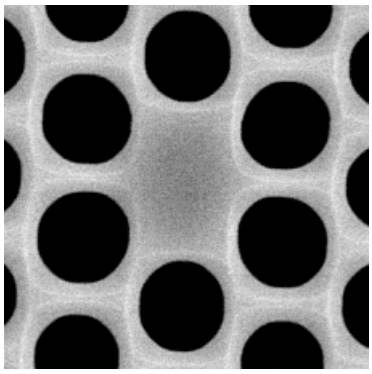

Fig. 7. SEM top view of the region around a missing etch pit after electrochemical pore growth and subsequent pore widening by oxidation/etching steps. The distance between the pores is 1.5 μm, the pore diameters are 1.15 μm [42].

a single missing pore. These missing pores disturb the translational symmetry of the periodic lattice and under appropriate conditions lead to localized states (microcavities) in the forbidden spectral region.

Chaining together such defects in, say, a line creates defect modes with transmission bands inside the photonic bandgap. As propagation is forbidden in the surrounding medium, according to theory waveguides with very sharp bends become possible.[6] In the past, we have analyzed different defect structures: linear[24] and bent waveguide, Y-branch, and microresonator[20] (Fig. 8). Here, we will discuss the impact of the linear defect on the optical properties of the structure in more detail.[24]

FD-TD calculations predict the occurrence of additional states throughout the entire range of the bandgap that are localized at the defect line. As we are experimentally coupling in from a plane wave, we may, however, only excite the states with even symmetry. The theoretical transmission spectrum for a straight waveguide is depicted in the upper part of Figure 9. For lower frequencies, single-mode transmission is expected. In addition, the waveguiding modes are partially reflected at the in- and the out-coupling facets and, therefore, lead to Fabry–Perot resonances. At higher frequencies a small gap is predicted where no states of even symmetry are available. Above the gap, states become available again, but they are so numerous that the resonances can no longer be resolved. The measured spectrum, which is shown in the lower part of Figure 9, shows remarkably good agreement with these predictions: While for low frequencies, single-mode resonances are observed, there is a well-pronounced stop band

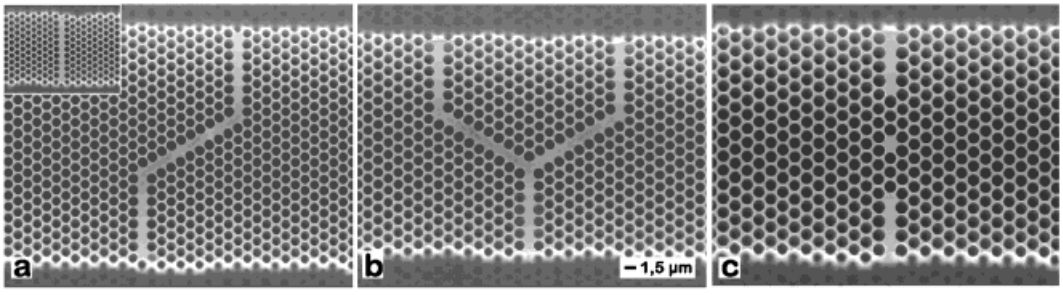

Fig. 8. Different defect structures realized in macroporous silicon with 1.5 μm interpore distance [42].

0935-9648/01/0603-0383 $ 17.50+.50/0

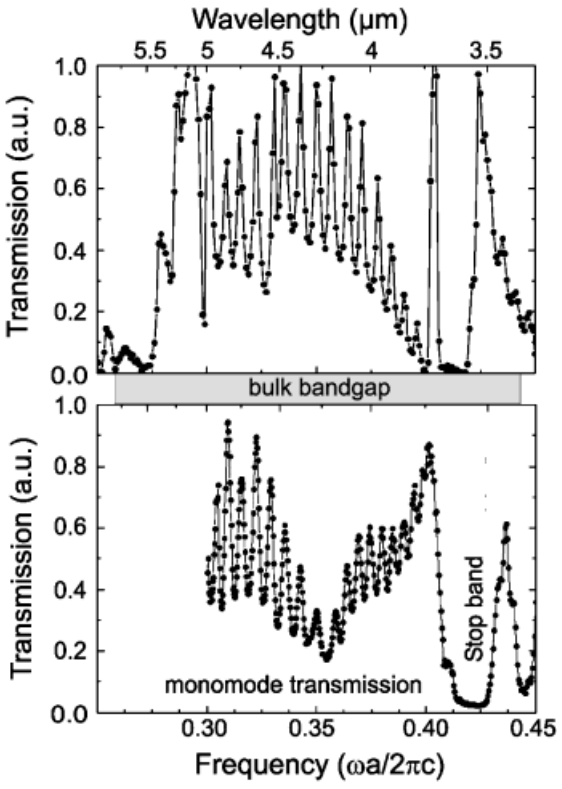

Fig. 9. Experimental transmission spectrum (bottom) of a linear waveguide structure compared to theoretical predictions (top). The bulk bandgap for H-polarization is marked by a gray bar [24].

and a broad transmission band at higher frequencies. Again, the small discrepancies between theory and experiment in the values of the finesse and stop band frequency can be explained by the strong influence of small deviations from the real dimensions to the values used in the calculation.

The observed high finesse results from the low coupling efficiency between the strongly localized waveguide modes and the external plane waves. In a realistic device the waveguide facets could be avoided by connecting other optical elements directly. These linear defects then act as almost ideal waveguides where the light is very well confined to within a few pore rows.

5. 3D Photonic Crystals

Band structure computations showed that for a face-centered cubic (fcc) lattice with a simple basis high dielectric inclusions in a low dielectric matrix do not yield a complete 3D bandgap, not even for an arbitrarily large dielectric contrast. The breakthrough came from the theoretical group at Iowa State University.[3] They discovered a complete photonic bandgap for an arrangement of photonic atoms in a diamond structure, an fcc structure with a two-atom basis, which lifts the polarization degeneracy of the one-atom fcc structure. A corresponding structure, which was manufactured by the group of Yablonovitch[25] and which is now known as "Yablonovite", was the first-fabricated photonic crystal that possessed a complete bandgap, albeit for microwave frequencies. The biggest disadvantage of a "Yablonovite" was that it could not be miniaturized easily. For instance, to obtain a complete photonic bandgap in the optical frequency range it would be necessary to accurately drill long channels less than 1 μm in diameter into a dielectric in a three-dimensionally ordered fashion.

One possibility has been proposed by Föll and co-workers.[26] They have observed that, in principle, macropores can also be used to realize 3D photonic crystal structures. In contrast to the macropores on (100) n-type substrates, which grow perpendicular to the substrate surface, pores on (111) substrates grow in the ⟨113⟩ crystalline direction. Since pores grow equally well in all three equivalent ⟨113⟩ directions a structure similar to the Yablonovite may be realized. A slight difference is that in these structures the pores are tilted about 29.5° off the vertical axis whereas in the Yablonovite they have an angle of about 35°. However, calculations from Klose and Dichtel[27] suggest that these structures should exhibit a complete 3D bandgap for an appropriate pore diameter. Föll and co-workers are currently trying to realize these structures by adjusting prepatterning techniques similar to those of the 2D macropore arrays. A disordered pore array, which does not exhibit a bandgap, can be seen in Figure 10.

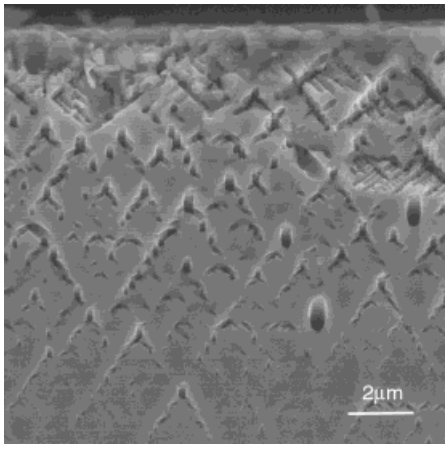

Fig. 10. Disordered 3D macroporous silicon photonic crystal obtained on (111) n-type Si ("Kielovite").

Another possibility for creating a 3D photonic crystal arises form the fact that, according to the established growth model of Lehmann[17,28] for pore formation, the current density at the pore tips is always equal to the critical current density j_{ps}. Therefore, the porosity p is determined by the ratio of the total current density to the critical current density. For a regular arrangements of cells with area A_{cell}, where all pores have the same area A_{pore}, the porosity is thus $p = A_{pore}/A_{cell} = j/j_{ps}$. The total current is controlled by the illumination intensity.

The scanning electron microscopy (SEM) cross-section image in Figure 11 demonstrates the quality of this etching process. The resulting samples have the expected strong asymmetrically varying pore shapes as defined by the current profile.

  0935-9648/01/0603-0384 $ 17.50+.50/0

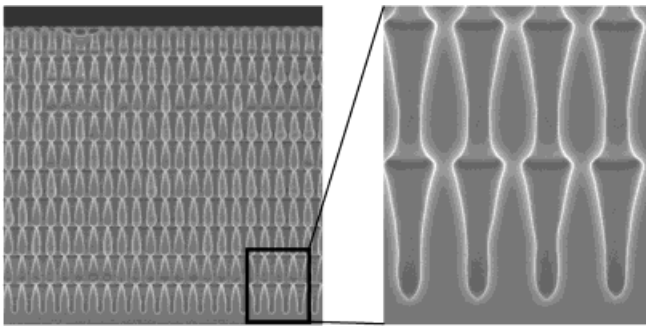

Fig. 11. SEM cross section of a sample etched with 10 periods of modulated light. The lattice constant l_{xy} in the xy-plane is 4.2 μm, in the z-direction l_z = 7.2 μm [29].

In the lateral direction, the sample is homogeneously etched over the whole exposed area without notable defects. With increasing pore depth the HF concentration at the pore tips and therefore also the critical current density j_{ps} as well as the etching speed v are reduced. If the sawtooth-like current density is applied on a linear time scale this leads to a strong variation of about 30 % in the length of a period from top to bottom for a 100 μm deep porous film. Using the reduction of growth speed from the homogeneous model of Lehmann[17] improves this effect dramatically. Up to 25 periods could be etched without notable deviation of the linear fit, leading to a total thickness of over 200 μm.[29] The transmission spectrum in the growth direction of the pores for a sample with a period of l_z = 7.2 μm is shown in Figure 12. Two strong stop bands can be observed near 320 cm^{-1} and 610 cm^{-1}. As the lateral

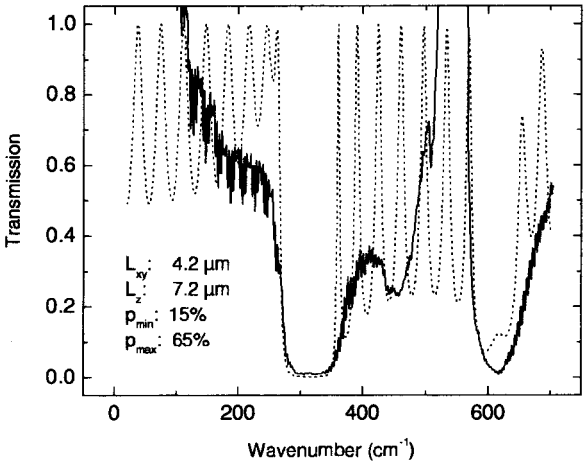

Fig. 12. Transmission spectrum for light travelling parallel to the pore axes (solid line) of the structure depicted in Figure 11 together with the calculated spectrum from a 1D Bruggeman approximation (dotted line). The lattice constant l_{xy} in the xy-plane is 4.2 μm, in the z-direction l_z = 7.2 μm. The porosity varies from p_{min} = 0.15 to p_{max} = 0.65 [29].

period is significantly smaller than the period in the growth direction, the optical behavior can, to a first approximation, be obtained by using an effective medium model. From the pore diameter, as measured from the SEM cross-section images, we determined the depth dependence of the porosity and then the effective refractive index using the Bruggeman formalism.[30] The calculated transmission spectrum for a multilayer model[31] using ten slabs for each period and eight periods in total is shown as a dotted line in Figure 12. The positions of the stop bands are well reproduced by this simple approximation. The Fabry–Perot-type interference pattern from the reflections at the front and back surfaces, which are very strong in the calculated spectrum, were not resolved in the experiment. The high transmission values around 550 cm^{-1} and below 180 cm^{-1} are artifacts due to the low background intensity of the spectrometer.

These samples demonstrate the ability to generate real 3D photonic crystals by modulating the backside illumination. Although the structures produced so far[32] do not exhibit a complete photonic bandgap, they have strongly nonlinear dispersion relations in all directions, behavior that will be very useful in nonlinear optical experiments. For instance, phase matching may easily be achieved in these structures, which for applications such as mixing experiments of beams with different wavelength may prove useful. In particular, the freedom to design the third, i.e., the z-direction, independently from the periodicity in the xy-plane will provide a very high flexibility.

Based on their initial studies of the diamond-like structures, the Iowa State group discovered another structure that is easier to miniaturize as the "Yablonovite", the so-called "Lincoln-log" structure.[33] This structure resembles a stack of wooden logs in parallel orientation to each other in each layer. Within each layer, SiO_2 was first deposited, patterned, and etched, such that two successive layers are oriented perpendicular to each other. The resulting trenches are then filled by poly-Si layers and finally the SiO_2 is removed completely. The second-nearest layers are displaced with respect to each other by half the bar distance within the layers. While the first of these crystals had a bandgap at a frequency of about 13 GHz (corresponding to a wavelength of about 2.3 cm), the recently fabricated crystals at Sandia National Laboratories[33] exhibit a bandgap at a wavelength of about 1.5 μm. However, the vertical extensions that have been achieved until now are rather small and the effort to produce large-scale 3D crystals will be substantial. The above-mentioned silicon Lincoln-log crystal,[33] for instance, consists of only five layers, i.e., 1.25 unit cells in the vertical direction. Instead of depositing each layer, Noda et al.[34] have applied wafer-bonding technology on III–V semiconductor substrates. This techniques allows multiplicative stacking, i.e., the preparation of a log structure similar to the one at Sandia National Laboratories, bonding two of these single-layer structures together, removing the substrate of the upper one, bonding two of those double-layer structures together, and so on (Fig. 13). Using this technique, a stack of eight layers has been achieved, corresponding to two units cells in the vertical direction.

Several research groups are pursuing a different approach to fabricating 3D photonic crystals: Under appropriate conditions, colloids self-organize into periodic structures that can extend over several hundred unit cells.[35] Due to their cubic symmetry, these crystals cannot possess a complete photonic bandgap, not even for the highest possible ratios of the indices

  0935-9648/01/0603-0385 $ 17.50+.50/0

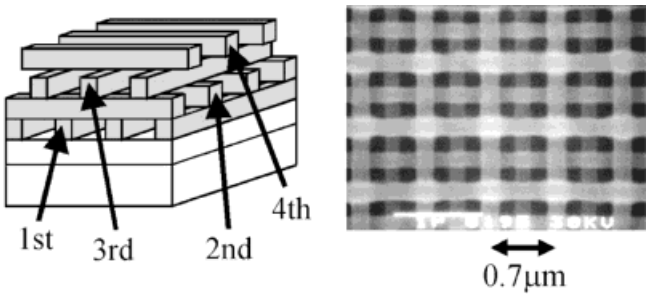

Fig. 13. Left: schematic drawing of one unit cell of the woodpile-structure 3D photonic crystal. Right: Top view SEM image of 3D photonic crystal prepared via the Noda approach. The lattice constant a is 0.7 μm, resulting in a bandgap around 1.3 μm [34].

of refraction $\eta = n_2/n_1$ of the constituent materials. However, the inverse structure, the so-called inverse opal, does have a complete bandgap in the higher bands.[5] A simplified recipe for the fabrication of inverse opals is as follows: Firstly, an artificial opal is fabricated, i.e., a close-packed fcc lattice of, for example, monodispersed SiO_2 spheres (diameter ranging from 100 to 1000 nm). The spheres are then sintered, making them shrink slightly and causing neighboring spheres to become firmly connected by a tube-like connection of SiO_2. Next, a high-index material is deposited into the void regions between the spheres. In a final step, in order to increase the dielectric contrast, the 3D network of SiO_2 spheres is removed by selective etching. This process may be called 3D templating. Very recently, the group at the University of Toronto reported the first successful fabrication of silicon-based inverse opals with a complete 5 % photonic bandgap relative to its center frequency for center frequencies at the telecommunication window around 1.5 μm.[36] Here, the voids of the artificial opal were almost completely filled with silicon by CVD. Figure 14

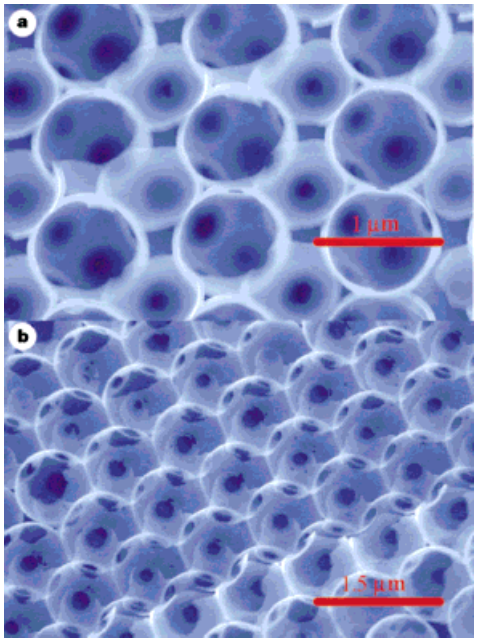

Fig. 14. SEM images of spatially periodic structures that have been obtained by infiltrating an artificial opal with silicon and subsequent removal of the opal. The lattice constant is 500 nm [36].

shows an SEM image of such a photonic crystal with a lattice constant of about 0.5 μm.

Using PWM (Sec. 1) it has recently been demonstrated theoretically[5] that it is possible to double the size of the inverse opal PBG by fine tuning the material's synthesis by, for example, careful sintering and control of the infiltration process. The resulting inverse opal structures (see Fig. 14) then consist of a high dielectric backbone with a filling ratio of about 25 %, leaving a large empty volume for infiltration by a low refractive index liquid crystal with strong optical anisotropy. This large volume of birefringent material makes the resulting system highly susceptible to electro-optic tuning effects. In particular, a change in the orientation of the nematic director field with respect to the inverse opal backbone by an external electric field can completely open or close the full, 3D PBG,[4] thus providing novel electro-optical ways to realize tunability of spontaneous emission, wave-guiding effects, and light localization. Recently, we have shown in collaboration with the University of Toronto for the first time as a proof of principle the feasibility of such an optical switch by introducing a liquid crystal into the pores of a 2D macroporous silicon photonic crystal and switching it thermally.[37]

6. Beyond Maxwell

Controlling the light propagation by photonic crystals opens entirely new avenues to applications outside the realm of classical electrodynamics, in particular in the fields of nonlinear optics as well as quantum optics. In order to fit within the scope of this overview article, we will discuss one example from each field.

Solitary waves are well known in various fields of physics: Solitary waves are solutions of nonlinear wave equations and can, for instance, be observed as step-shaped waves running down slightly inclined streets during heavy rain. A defining characteristic of solitary waves is that they do not change their shape during propagation—they are free of dispersion. In a nonlinear dielectric, i.e., a dielectric with an intensity-dependent index of refraction, it is possible that the dispersion- induced decay of a wave packet during propagation may be compensated by self-focussing effects. In this case, a solitary wave forms. The time stability of this type of wave makes it particularly promising as an information carrier, since using solitary waves one can send signals with extremely high pulse rates over long distances without fearing scrambling of successive pulses.

For some time now a slightly different kind of solitary wave, the so-called gap soliton, has been studied in 1D photonic crystals. Here, one starts with a pulse the central frequency of which lies within the bandgap of a photonic crystal. Due to an intensity-dependent index of refraction of at least one of the components of the crystal, an energetic pulse can distort the local band structure to such an extent that it causes the central frequency of the pulse to lie outside the bandgap. While it propagates, a sufficiently energetic pulse forms its own channel of transmission. In contrast to that, however, the investiga-

  0935-9648/01/0603-0386 $ 17.50+.50/0

ADVANCED MATERIALS

tion of gap solitons in 2D or 3D photonic crystals is still in its infancy, yet promises to yield a wealth of interesting phenomena. Compared to 1D structures, the photonic band structure of higher dimensional crystals offers qualitatively new properties. For instance, the bandgap along one high-symmetry direction may be slightly shifted and the corresponding modes of the photonic crystals may have different symmetries. This leads to quite a number of solitary wave types with various threshold intensities as well as propagation speeds.[38] Consequently, one might use one solitary wave as a switch for another one or gate one solitary wave with the other one. In this respect, one could consider the first solitary wave some sort of "ice-breaker" for the second one. By modifying the intensity in the dielectric, the first solitary wave creates a channel through the "ice" of the photonic bandgap, which the second solitary wave could not enter before. The direction of the channel is then determined by the first solitary wave. Since the ice-channel in this Gedanken experiment freezes on the timescale of picoseconds, one is dealing here with an ultrafast phenomenon.

Quantum optics is another field in which photonic crystals offer qualitatively new possibilities: In a nutshell, the tailoring of the photonic density of states by means of photonic crystals allows far-reaching control of the emission characteristics of corresponding color centers. In illustration of this we discuss the qualitative behavior of an idealized two-level atom in a photonic crystal. If the transition frequency is well within a complete photonic bandgap, the atom cannot decay to its ground state via a one-photon process. A bound photon–atom state is formed instead. Furthermore, calculating the atomic relaxation via an allowed two-photon process for atomic resonance frequencies within a complete photonic bandgap[39] yields lifetimes of several days. Due to the idealization typical of quantum-optical calculations, this lifetime for real systems is certainly too long. However, it can be assumed that the lifetimes of excited atoms or molecules in suitable photonic crystals exceed the corresponding ones in vacuum by several orders of magnitude. This possibility of controlling the spontaneous emission via the tailored density of states alone would be of paramount importance to the achievement of novel quantum-optical effects.

Particularly interesting phenomena occur for frequencies near the edge of a photonic bandgap. In this frequency range, the dispersion relation decreases remarkably (see Fig. 1a), which leads to a very low group velocity, causing the photon–atom interaction to increase. For simplicity, the discussion is restricted to an atom with an excited and a ground state, $|c\rangle$ and $|g\rangle$, respectively, as well as to two corresponding states of the electromagnetic field mode with no and one photon, $|0\rangle$ and $|1\rangle$, respectively. By analogy with the formation of a "binding" as well as an "antibinding" state for the ammonium molecule, due to the strong interaction between the atom and the field the "bare" atomic eigenstates form combined atom–field eigenstates, which in quantum optics are referred to as "dressed states". In order to understand the dynamical behavior of an initially excited atom one has to imagine a decomposition of this initial state into linear combinations of the states that form the Rabi-duplett, which themselves, due to the splitting of their energy levels, evolve differently with time. As the photon remains in an ideal cavity, i.e., in our case the photonic bandgap, the wavefunction of the photon–atom system will oscillate between the states of the Rabi-duplett. If the "bare" atomic transition frequency is in close proximity to a photonic band edge, but still just within the photonic bandgap, the Rabi splitting may become so large that one component of the Rabi-duplett will be pushed outside the photonic bandgap into the photonic conduction band. In contrast to its partner, this state thus acquires a finite lifetime by being coupled with the photonic conduction band. As the initially excited atom may decay "partially", so-called fractional localization occurs.[39,40] Figure 15 shows the relaxation behavior of an excited two-level atom as a function of the position of the bare transition frequency relative to the photonic band edge. A detailed explanation is given in the literature.[40]

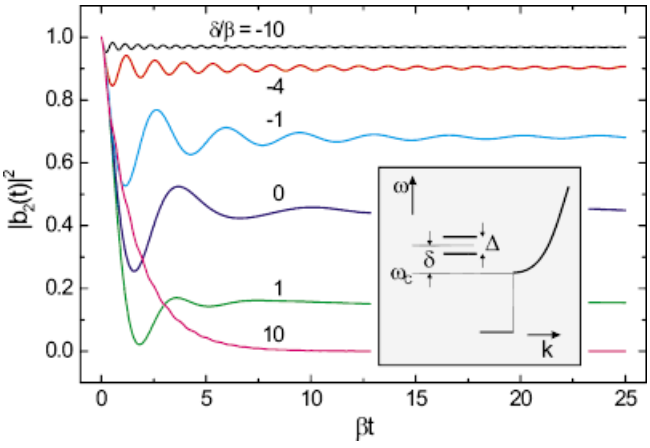

Fig. 15. Temporal evolution of the occupation $|b_2(t)|^2$ of the upper level of an initially excited two-level atom for various values of its transition frequency $\omega_{21} = \omega_c + \delta$ relative to the band edge at ω_c. The photonic conduction band lies at frequencies $\omega > \omega_c$. Characteristic are the damped Rabi oscillations and the finite oscillator amplitude for long times, which correspond to the "partial" decay of the excited level. The fractional localization drops from nearly 1 (far below the band edge in the bandgap) to 0 (in the band).

One may imagine the above situation in terms of an excited atom which emits a photon that, due to the strong Bragg scattering at frequencies near the band edge, finds its way back to the atom where it is reabsorbed. This photon feedback effect makes the atom develop a memory of its previous state. Such and similar memory effects are not limited to band edges but occur wherever the photon density of states changes abruptly.

If only one single excited atom exhibits such a peculiar behavior in a photonic crystal, one is tempted to speculate about the behavior of multi-level atoms, of atoms resonantly driven by laser fields and, finally, about the collective behavior of several atoms embedded in a photonic crystal. Currently, aspects such as the so-called band edge laser are the subject of intense research efforts and discussing them here would certainly go beyond the scope of this review article.[41]

  0935-9648/01/0603-0387 $ 17.50+.50/0

7. Conclusions and Outlook

There exists a strong analogy between electrons in semiconductor crystals and photons ("light particles") in photonic crystals: Multiple scattering at periodically positioned "dielectric atoms" leads to the formation of an optical band structure. Under certain circumstances optical bandgaps form, which fundamentally alter light propagation as well as emission processes of active atoms in these artificial structures. This rather new knowledge gained about one decade ago has triggered intensive research efforts that initially focused on fundamental research on how to "make light stand still". Novel integrated photonic devices have been proposed that, through their miniaturization and high efficiency, could open the door to entirely new classes of all-optical devices. Recent progress in nanofabrication makes it possible that photonic bandgap devices will be realized in the near future, potentially signaling the start of a photonic revolution comparable to the semiconductor revolution, which began half a century ago.

We have reviewed recent progress on 2D photonic crystals based on macroporous silicon in particular. Transmission measurements on bulk and finite macroporous silicon photonic crystals show good agreement with theoretical predictions for a wide range of pore diameters. The lattice constants can be varied in the range from 8000 down to 500 nm, resulting in complete bandgaps in a wavelength range between 20 and 1.3 μm. Passive devices such as waveguides and microresonators have been fabricated and optically characterized, showing good agreement between theoretical calculations and measured transmission spectra. Also first active devices based on liquid-crystal infiltrated macropores have been produced. Periodicity in the third direction can be achieved either by modulating the macropore diameter or by the "Kielovite" technique. The precision of the achieved samples and the presented optical data prove the suitability of electrochemically etched macroporous silicon as a candidate for new optical devices based on photonic crystals in the near and mid infrared spectral range.

Received: August 21, 2000

[1] A. R. Parker, R. C. McPhedran, D. R. McKenzie, L. C. Botten, N. A. P. Nicorovici, *Nature* **2001**, *409*, 36.
[2] *Photonic Bandgap Materials* (Ed: C. M. Soukoulis), Kluwer, Dordrecht, The Netherlands **1996**. *Photonic Crystals* (Eds: J. D. Joannopoulos, R. D. Meade, J. N. Winn), Princeton Academic Press, Princeton, NJ **1995**.
[3] K.-M. Ho, C. T. Chan, C. M. Soukoulis, *Phys. Rev. Lett.* **1990**, *65*, 3152.
[4] K. Busch, S. John, *Phys. Rev. Lett.* **1999**, *83*, 967.
[5] K. Busch, S. John, *Phys. Rev. E* **1998**, *58*, 3896.
[6] A. Mekis, J. C. Chen, I. Kurland, S. Fan, P. R. Villeneuve, J. D. Joannopoulos, *Phys. Rev. Lett.* **1996**, *77*, 3787.
[7] M. Sigalas, C. M. Soukoulis, E. N. Economou, C. T. Chan, K. M. Ho, *Phys. Rev. B* **1993**, *48*, 14 121.
[8] R. C. McPhedran, L. C. Botten, A. A. Asatryan, N. A. Nicorovici, P. A. Robinson, C. M. de Sterke, *Phys. Rev. E* **1999**, *60*, 7614.
[9] V. Yannopaps, N. Stefanou, A. Modinos, *J. Phys.: Condens. Matter* **1997**, *9*, 10 261.
[10] B. G. Bovard, *Appl. Opt.* **1993**, *32*, 5427.
[11] M. G. Berger, R. Arens-Fischer, M. Thoenissen, M. Krueger, S. Billat, H. Lueth, S. Hilbrich, W. Theiss, P. Grosse, *Thin Solid Films* **1997**, *297*, 237.
[12] D. N. Chigrin, A. V. Lavrinenko, D. A. Yarotsky, S. Gaponenko, *Appl. Phys.* **1999**, *68*, 25.
[13] J. S. Foresi, P. R. Villeneuve, J. Ferrera, E. R. Thoen, G. Steinmeyer, S. Fan, J. D. Joannopoulos, L. C. Kimerling, H. I. Smith, E. P. Ippen, *Nature* **1997**, *390*, 143.
[14] V. Lehmann, *J. Electrochem. Soc.* **1993**, *140*, 2836. A. P. Li, F. Müller, A. Birner, K. Nielsch, U. Gösele, *J. Appl. Phys.* **1998**, *84*, 6023.
[15] U. Grüning, V. Lehmann, S. Ottow, K. Busch, *Appl. Phys. Lett.* **1996**, *68*, 747. U. Grüning, V. Lehmann, U. Eberl, *Phys. Bl.* **1996**, *52*, 661.
[16] V. Lehmann, H. Föll, *J. Electrochem. Soc.* **1990**, *137*, 653.
[17] V. Lehmann, *J. Electrochem. Soc.* **1993**, *140*, 2836.
[18] A. Birner, U. Grüning, S. Ottow, A. Schneider, F. Müller, V. Lehmann, H. Föll, U. Gösele, *Phys. Status Solidi A* **1998**, *165*, 111.
[19] S. Ottow, V. Lehmann, H. Föll, *J. Electrochem. Soc.* **1996**, *143*, 385.
[20] A. Birner, A.-P. Li, F. Müller, U. Gösele, P. Kramper, V. Sandoghdar, J. Mlynek, K. Busch, V. Lehmann, *Mater. Sci. Semicond. Proc.* **2000**, *3*, 487.
[21] J. Schilling, A. Birner, F. Müller, R. B. Wehrspohn, R. Hillebrand, U. Gösele, K. Busch, S. John, S. W. Leonard, H. M. van Driel, *Opt. Mater.*, in press.
[22] S. Rowson, A. Chenokov, C. Cuisin, J.-M. Lourtioz, *IEEE Proc.—Optoelectron.* **1998**, *145*, 403.
[23] S. W. Leonard, H. M. van Driel, K. Busch, S. John, A. Birner, A.-P. Li, F. Müller, U. Gösele, V. Lehmann, *Appl. Phys. Lett.* **1999**, *75*, 3063.
[24] S. W. Leonard, H. M. van Driel, A. Birner, U. Gösele, P. R. Villeneuve, *Opt. Lett.* **2000**, *25*, 1550.
[25] E. Yablonovitch, T. J. Gmitter, K. M. Leung, *Phys. Rev. Lett.* **1991**, *67*, 2295.
[26] M. Christophersen, J. Carstensen, A. Feuerhake, H. Föll, *Mater. Sci. Eng. B* **2000**, *69*, 194.
[27] R. Klose, K. Dichtel, unpublished results.
[28] V. Lehmann, U. Grüning, *Thin Solid Films* **1997**, *297*, 13.
[29] F. Müller, A. Birner, J. Schilling, U. Gösele, C. Kettner, P. Hänggi, *Phys. Status Solidi A* **2000**, *182*, 585.
[30] D. A. G. Bruggeman, *Ann. Phys. (Leipzig)* **1935**, *24*, 636.
[31] F. Abelès, *Ann. Phys. (Paris)* **1950**, *5*, 596.
[32] J. Schilling, F. Müller, S. Matthias, R. B. Wehrspohn, U. Gösele, K. Busch, *Appl. Phys. Lett.* **2001**, *78*, 1180.
[33] S. Y. Lin, J. G. Fleming, D. L. Hetherington, B. K. Smith, R. Biswas, K. M. Ho, M. M. Sigalas, W. Zubrzycki, S. R. Kurtz, J. Bur, *Nature* **1998**, *394*, 251.
[34] S. Noda, N. Yamamot, M. Imada, H. Kobayashi, M. Okano, *J. Lightwave Technol.* **1999**, *17*, 1948.
[35] W. L. Vos, R. Sprik, A. van Blaaderen, A. Imhof, A. Laghendijk, G. H. Weydam, *Phys. Rev. B* **1996**, *53*, 16 231.
[36] A. Blanco, E. Chomski, S. Grabtchak, M. Ibisate, S. John, S. W. Leonard, C. Lopez. F. Meseguer, H. Miguez, J. P. Mondia, G. A. Ozin, O. Toader, H. M. van Driel, *Nature* **2000**, *405*, 437.
[37] S. W. Leonard, J. P. Mondia, H. M. van Driel, O. Toader, S. John, K. Busch, A. Birner, U. Gösele, V. Lehmann, *Phys. Rev. B* **2000**, *61*, R2389.
[38] N. Aközbek, S. John, *Phys. Rev. E* **1998**, *57*, 2287.
[39] S. John, J. Wang, *Phys. Rev. Lett.* **1990**, *64*, 2418. *Phys. Rev. B* **1991**, *43*, 12 722.
[40] S. John, T. Quang, *Phys. Rev. A* **1994**, *50*, 1764.
[41] S. John, T. Quang, *Phys. Rev. Lett.* **1996**, *76*, 2484. *Phys. Rev. Lett.* **1997**, *78*, 1888. T. Quang, M. Woldeyohannes, S. John, G. S. Agarval, *Phys. Rev. Lett.* **1997**, *79*, 5238. N. Vats, S.John, *Phys. Rev A* **1998**, *58*, 4168. M. Woldeyohannes, S. John, *Phys. Rev. A* **1999**, *66*, 5046.
[42] F. Müller, A. Birner, U. Gösele, V. Lehmann, S. Ottow, H. Föll, *J. Porous Mater.* **2000**, *7*, 201.

  0935-9648/01/0603-0388 $ 17.50+.50/0